Environ. Sci. Technol. **2010,** *44,* 3238–3244

Hydrogen Peroxide Photocycling in the Gulf of Aqaba, Red Sea

YEALA SHAKED,*,†,‡ RAVIV HARRIS,† AND NIR KLEIN-KEDEM†

Interuniversity Institute for Marine Sciences, Eilat, 88103, Israel, and Institute of Earth Sciences, The Hebrew University, Jerusalem, 91904, Israel

Received August 6, 2009. Revised manuscript received March 2, 2010. Accepted March 8, 2010.

The dynamics of hydrogen peroxide (H_2O_2) was investigated from December 2007 to October 2008 in the Gulf of Aqaba, which in the absence of H_2O_2 contribution from biological production, rain and runoff, turned out to be a unique natural photochemical laboratory. A distinct seasonal pattern emerged, with highest midday surface H_2O_2 concentrations in spring−summer (30−90 nM) as compared to winter (10−30 nM). Similarly, irradiation normalized net H_2O_2 formation rates obtained in concurrent shipboard experiments were faster in spring−summer than in winter. These seasonal patterns were attributed to changes in water characteristics, namely elevated spring−summer chromophoric dissolved organic matter (CDOM).

The role of trace elements in H_2O_2 photoformation was studied by simultaneously measuring superoxide (O_2^-), Fe(II), and H_2O_2 formation and loss in ambient seawater and in the presence of superoxide dismutase, iron and copper. O_2^- was found to decay fast in the Gulf water, with a half-life of 15−28 s, primarily due to catalytic reactions with trace metals (predominantly copper). Hence, H_2O_2 formation in the Gulf involves metal-catalyzed O_2^- disproptionation. Added iron moderately lowered net H_2O_2 photoformation, probably due to its participation in Fe(II) oxidation, a process that may also modify H_2O_2 formation in situ.

Introduction

Hydrogen peroxide (H_2O_2) and its precursor superoxide ion radical (O_2^-) are reactive oxygen species that play a central role in a variety of important biogeochemical processes occurring in seawater. They react with and can be significantly involved in the cycling of dissolved organic matter, trace metals and a number of highly reactive free radicals (*1*−*4*). H_2O_2 is a relatively stable intermediate with a half-life ranging from a few hours in lakes and coastal environments to a few days in open ocean oligotrophic waters (*3, 5, 6*). For the most part it decays due to biological/enzymatic degradation and redox reactions with reduced metals (*5*−*8*). H_2O_2 concentrations in seawater range from below detection limit (sub nanomolar) to 300−500 nM, depending on the trophic state of the seawater (eutrophic to oligotrophic), on location (open-sea, coastal, or estuarine waters), on water depth and on the diurnal cycle (*3, 5, 9*−*13*). There are several potential sources that deliver H_2O_2 to surface seawater including in situ photochemical formation, biological activity, wet (rain), and dry atmospheric deposition, and redox cycling of metals (*1*−*3, 6*−*15*).

Photochemical reactions involving chromophoric dissolved organic matter (CDOM) and solar irradiance (mostly in the UV range) have been suggested as the main pathways for H_2O_2 formation in natural waters (*1, 3, 9, 15*). It is thought that in these reactions, photochemically excited CDOM molecules transfer electrons to dissolved O_2 and generate superoxide (O_2^-):

$$\mathrm{CDOM} + \mathrm{O_2} \xrightarrow{h\nu} \mathrm{CDOM_{ox}^+} + \mathrm{O_2^-} \quad (1)$$

Superoxide then decays by autoredox biomolecular dismutation, referred to hereafter as uncatalyzed dismutation (*16*):

$$\mathrm{HO_2} + \mathrm{O_2^-}(+\mathrm{H^+}) \rightarrow \mathrm{H_2O_2} + \mathrm{O_2} \quad (2)$$

In seawater, uncatalyzed O_2^- dismutation will take place only when O_2^- concentrations are higher than those of redox reactive trace metals such as iron and copper (*16, 17*). Hence, in many marine environments reactions between superoxide, trace metals and organic matter (including the enzyme superoxide dismutase, SOD) may predominate over the uncatalyzed disproportionation (*16*−*20*). Reactions with dissolved metal ions are especially interesting because of their potential for generating measurable concentrations of these metals in unstable oxidation states:

$$\mathrm{M^{n+}} + \mathrm{O_2^-}(+2\mathrm{H^+}) \rightarrow \mathrm{M^{n+1}} + \mathrm{H_2O_2} \quad (3)$$

$$\mathrm{M^{n+1}} + \mathrm{O_2^-} \rightarrow \mathrm{M^{n+}} + \mathrm{O_2} \quad (4)$$

When O_2^- acts both as an oxidant (eq 3) and as a reductant (eq 4), a redox cycle is established that catalyzes the dismutation of O_2^- (similar to SOD and some organic molecules *16, 17, 19*). A catalytic redox cycle would produce a stoichiometry of 0.5 H_2O_2 per O_2^- and a pseudo first order decay of O_2^- (*16, 18*). However, when O_2^- acts only as an oxidant or as a reductant, a resulting stoichiometry of 1 or 0 H_2O_2 per O_2^- respectively is expected, and O_2^- decay will not follow pseudofirst order (providing the initial concentration of O_2^- approaches those of the metals (*18*)). In seawater at subnanomolar O_2^- concentrations (*21*), the far more abundant oxygen and H_2O_2 (10^5 and 10^3 times higher respectively) may compete with O_2^- for the oxidation of reduced metals (mostly iron) through reactions 5 and 6:

$$\mathrm{M^{n+}} + \mathrm{O_2} \rightarrow \mathrm{M^{n+1}} + \mathrm{O_2^-} \quad (5)$$

$$\mathrm{M^{n+}} + \mathrm{H_2O_2} \rightarrow \mathrm{M^{n+1}} + \mathrm{OH} + \mathrm{OH^-} \quad (6)$$

In such a scenario, a metal catalyzed O_2^- dismutation may not occur (depending on the reaction rates of the individual reactions), and additional O_2^- production (eq 5) and/or H_2O_2 consumption (eq 6) may take place (*2, 20, 21*). By examining both the stochiometry of H_2O_2 and O_2^- formation and the decay kinetics of O_2^-, we can determine which reactions lead to H_2O_2 formation and assess the relative role of O_2^- as a reductant and as an oxidant in natural waters (*15, 16, 18*).

The arid, always sunny, oligotrophic Gulf of Aqaba, is a unique and (highly) accessible natural laboratory where the photocycling of reduced oxygen species (H_2O_2 and O_2^-) and reduced metals can be studied at high temporal and spatial resolution (*22*). As part of a larger research effort attempting to link the photochemical transformations of oxygen radicals

* Corresponding author phone: 972-8-6360139; fax: 972-8-6374329; e-mail: yshaked@vms.huji.ac.il.
† Interuniversity Institute for Marine Sciences.
‡ The Hebrew University.

10.1021/es902343y

Published on Web 04/08/2010

TABLE 1. Surface H_2O_2 Concentrations, On Board Net H_2O_2 Formation Rates, UV Flux, Surface Iron Concentrations and CDOM Absorbance Measured during the Study Period

	surface $[H_2O_2]$[a]		on board H_2O_2 formation		UV flux	surface [Fe][c]		CDOM[e]
	daily max nM	noon ave nM	net rate nM h^{-1}	UV norm net rate[b] nM m^2 W^{1-} h^{-1}	integrated[d] W h m^{-2}	dissolved nM	total nM	α355 m^{-1}
Winter								
18-Dec-07	30	21	55	2.3	72	4.3	7.8	
17-Jan-08	23	16	44	2.0	88	3.8	7.6	0.079
12-Feb-08	26	20	51	2.0	107	5.6	11.8	
18-Mar-08	32	28	77	2.4	125	3.9	8.2	0.084
Spring and Summer								
14-Apr-08	75	46	116	3.4	151	5.0	6.9	0.092
28-Apr-08[f]	107	78	218	5.9	184			0.078
30-Apr-08[f]	104	86			183			0.094
01-May-08[f]	79	57			182			0.110
12-May-08	25	32	78	2.5	73	4.6	11.0	0.109
15-Jun-08	109	66	230	5.6	189	5.4	11.5	0.087
09-Jul-08	88	80	217	5.7	181	contamin	9.4	0.149
19-Aug-08	43	41			157	4.5	9.3	0.110
16-Sep-08	64	50	147	4.4	159	5.1	6.8	0.119
27-Oct-08	42	36	103	4.8	118	4.1	6.1	
Comparison between the Seasons								
winter Ave[g]	28	22	57	2.2	98	4.4	8.8	0.0813
winter SD[h]	*4.0*	*5.1*	*14*	*0.23*	*23*	*0.82*	*2.0*	*0.0031*
spring−summer Ave[g]	74	57	158	4.6	158	4.8	8.7	0.105
spring−summer SD[h]	*30*	*19*	*63*	*1.3*	*37*	*0.49*	*2.1*	*0.0211*
t -test *p* value[i]	*0.0008*	*0.0002*	*0.0045*	*0.0024*	*0.005*	*0.431*	*0.914*	*0.0096*

[a] Surface H_2O_2 concentrations are presented as daily maxima and averages of 3−5 discrete measurements conducted around noon (between 11:00−13:00). [b] UV normalized net H_2O_2 formation rates obtained by plotting $[H_2O_2]$ versus accumulated UV flux, see SI Figure S4. [c] Dissolved (<0.2 μm) and total iron of duplicate samples from 20 m (SD < 20%). [d] Solar fluxes integrated from first light to high noon. The UV fraction was calculated based on the calibrations presented in SI Table S2 (4.2% of the global irradiation). [e] Absorption coefficient α355 of chromophoric dissolved organic matter (CDOM) from absorption measurements at 355 nm (see Materials and Methods). [f] Sampled off the IUI pier as part of the high resolution diurnal cycle (see SI, Figure S2) [g] Averages. [h] Standard deviations on the averages. [i] Statistical test for seasonal differences in the measured parameters (considered significant when *p* value < 0.05). Student *t* test, two tailed unpaired, two-sample unequal variance (heteroscedastic).

and trace elements in this environment, we set out to characterize H_2O_2 dynamics throughout the year. We combine multiple measurements and experiments from recurrent cruises to identify seasonal patterns and single out the parameters driving them. Additionally, we examine the role of trace elements in H_2O_2 photoformation by recording the dynamics of superoxide, Fe(II) and H_2O_2 in naturally irradiated experiments with ambient seawater and in the presence of the enzyme superoxide dismutase (SOD), iron and copper.

Materials and Methods

Water Sampling and On-Board Experiments. Fourteen day-long sampling campaigns were conducted between December 2007 and October 2008 in the northern Gulf of Aqaba (Tables 1 and Supporting Information (SI) S1). Most campaigns were carried out in an open water station (St. A, 29.46°N, 34.93°E; SI Figure S1) in conjunction with the Israel National Monitoring Program (NMP) monthly cruises. In each cruise, surface $[H_2O_2]$ was examined throughout the day and in summer its vertical distribution was studied around midday (between 11:00 and 13:00). Detailed, three day long, H_2O_2 diurnal cycles were measured in spring 2008 off the Inter-university Institute for Marine Sciences in Eilat (IUI) pier (SI Figure S2). On-board experiments with freshly collected seawater were carried out in all cruises around midday. These are regarded as maximal net H_2O_2 production rates, which aid in examining the seasonal H_2O_2 dynamics, but are higher than the typical 10−25 nM hr^{-1} net formation rates typical of in situ incubated quartz tubes (see SI for more details).

Simultaneous determination of O_2^-, Fe(II) and H_2O_2 photodynamics. Additional H_2O_2 photoexperiments were conducted on-shore under natural irradiation, in 1 L acid cleaned Pyrex beakers, which were sampled also for O_2^- and Fe(II). Tested treatments included ambient seawater (with 4−6 nM dissolved Fe and ~2 nM dissolved Cu), added Fe (15 and 30 nM) and added Cu (3 and 6 nM), both of which were pre-equilibrated for three hrs. Samples for H_2O_2 were collected every 20−30 min, kept on ice in the dark and analyzed together using Amplex UltraRed fluorometery. H_2O_2 dark formation and post illumination decays were followed for all treatments. During the experiment 2−4 runs of O_2^- and Fe(II) dynamics were conducted for each treatment with the FeLume system operated in continuous mode with MCLA or Luminol, respectively. In each such run, the $[O_2^-]_{s.s}$ or $[Fe(II)]_{s.s}$ of an illuminated sample was measured first, then $Fe(II)/O_2^-$ decay in a covered sample was recorded, and finally their photoformation was examined by re-exposing the sample to the sun. To properly describe these fast reactions high flow rates (5 mL min^{-1}) and frequent data acquisition (4 readings sec^{-1}) were adapted. The FeLume signal was converted to concentrations using slightly acidic Fe(II) spikes (*22*) and photochemically produced O_2^- spikes (SI Figure S8), with which the various O_2^- sinks were also assessed (Figure 2). The FeLume configurations and chemistry details are provided in the SI.

Hydrogen Peroxide Analysis. Hydrogen peroxide was measured with a Varian spectrophotometer (Cary 50) or a Varian spectrofluorometer (Cary Eclipse) according to the Amplex UltraRed based technique of Zhou et al. (*23*). Principally, H_2O_2 in the presence of horseradish peroxidase reacts with Amplex UltraRed at a 1:1 stoichiometry to produce fluorescent resorufin, which can be determined spectrophotometrically at 568 nm (ε = 57 000 M^{-1} cm^{-1}) or fluorometrically (λ_{ex} = 560 nm, λ_{em} = 580 nm). Frequent

analysis of duplicate samples in both instruments assured greater reproducibility and accuracy needed for the time series measurements. The reagent stock consists of 200 μM Amplex UltraRed and 100 kU L^{-1} horseradish peroxidase, added at a 1:100 dilution. H_2O_2 concentrations were determined by the standard additions method, with three to five additions of freshly diluted H_2O_2 standards to replicate subsamples. The diluted standards were made from a stock peroxide solution (1 mM) that was prepared daily from 30% (w/w) H_2O_2 (Suprapur, Merck) and checked for stability using UV absorbance at 240 nm ($\varepsilon = 38.1\ M^{-1}\ cm^{-1}$). The method blank was determined in catalase amended seawater (Sigma, 25U/ml and 1 h reaction time). Detection limit, defined as three times the blank SD, was typically 5 nM (ranged between 1 and 15 nM) and the error on replicate analysis was 10−15%.

Analysis of Associated Parameters. CDOM absorption coefficient was obtained in 0.2 μm filtered seawater using a Varian double beam UV−vis spectrophotometer (Cary 300) and a 5 cm or 10 cm rectangular quartz cell. All spectra were referenced against Milli *Q* water. The absorption coefficient at 355 nm (a355) was calculated from seawater absorbance spectra according to Kirk (*24*). Iron sampling and analysis protocols are outlined in Shaked (*22*). Briefly, total and dissolved (<0.2 μm) samples were acidified with distilled HCl to pH ~ 1.7 and kept for 6 months prior to reduction with sulfite and direct analysis in the FeLume system. Meteorological data were collected continuously at the IUI pier. Solar irradiance in the air was measured with a whole hemisphere (180° field of view) CM11B Pyranometer (Kipp and Zonen), located 7 m above the water, with a spectral range of 310 to 2800 nm. Extensive calibrations between the pyranometer and two radiometers were carried out to enable the conversion of the global irradiation data to the photochemically relevant UV data (Table S2). Complementary hydrographic, chemical, and biological measurements were conducted by the Israeli NMP monitoring program (Tables 1 and SI S1).

Results and Discussion

H_2O_2 Dynamics in the Gulf of Aqaba. *Photochemistry as a sole source of H_2O_2.* Our field measurements and experiments all show that photochemical processes are solely responsible for H_2O_2 production in the Gulf of Aqaba. In all but one cloudy cruise (Feb 08), a build-up in surface [H_2O_2] followed by a late afternoon decline was found (Figure 1a, and SI Figures S2 and S3). These data agree with former measurements in the Gulf (*25*) and other subtropical ocean regions (*10*−*13*). The depth distribution of H_2O_2, studied in detail in the summer months also shows photochemically typical behavior with surface maxima followed by an exponential decline with depth (Figure 1b). In this highly arid environment H_2O_2 contribution from rain or runoff is unimportant, leaving biological H_2O_2 production as a single potential source in addition to photochemistry. Nonetheless, we found no evidence for significant biological H_2O_2 production either in the depth profiles that show no feature associated with the chlorophyll-*a* maximum (Figure 1b) nor in 12 h incubations of natural and algal enriched spring waters (from 20 m, 30 fold enrichment by gentle filtration on 0.2 μm membrane).

Seasonality in H_2O_2 Concentrations and Net Formation and Their Driving Factors. A distinct seasonal pattern in surface H_2O_2 concentrations was found with lower concentrations of 10−30 nM in winter (December−March) and higher concentrations of 30−90 nM in spring−summer (April−October; Table 1, SI Figure S3). Since surface H_2O_2 changes during the day, we compared the daily maximum and the average noon concentrations (represents 3−4 samples measured between 11:00 and 13:00), both of which were 2.6 fold higher during spring−summer than in winter (Table 1). In addition, the on-board experiments revealed higher net H_2O_2 photoformation rates in spring−summer

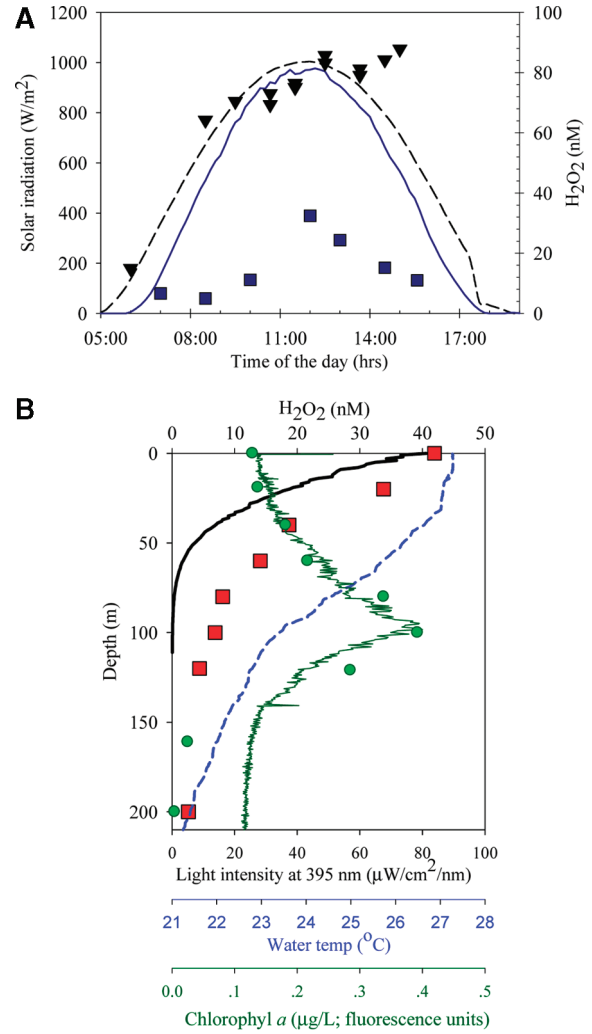

FIGURE 1. Temporal and spatial distribution of H_2O_2 in representative cruises. (A). Diel patterns of H_2O_2 in surface waters in March (squares) and July 2008 (triangles) and corresponding solar irradiation intensities (March, solid line; July, dashed line). (B) H_2O_2 depth profile (squares) measured at midday in August 2008 when thermal stratification prevails, as shown by the sharp temperature (dashed blue line) gradient. Also shown are the long UV, 395 nm irradiation profile (solid black line) and chlorophyll *a* profile measured by an in-situ fluorometer (green line) and in extracted samples (green circles).

compared to winter (Table 1, p value = 0.0045). The higher irradiation intensities and longer daylight hours characterizing the transition from winter to spring−summer warm up the surface layers and lead to the development of a stable thermocline (SI Table S1). These conditions (and the high nutrient concentrations in the waters) favor the commencement of a phytoplankton spring bloom (SI Table S1), which is a likely source of chromophoric dissolved organic matter (CDOM). Seasonal changes in other factors such as solar spectrum, downward mixing, H_2O_2 decomposition rates, and trace metal concentrations and reactivity may also influence these patterns. Below we outline the data and approaches taken to assess the relative roles of various environmental parameters in determining H_2O_2 seasonality, a framework into which we tie our current understanding of H_2O_2 dynamics in the Gulf of Aqaba.

Solar Irradiation. While evidently less H_2O_2 was formed on cloudy days (e.g., May 12th, Table 1), seasonal variations in the solar irradiation intensity were too small to explain the distinct winter to spring−summer change in surface H_2O_2

concentrations (sunrise to noon integrated solar fluxes vary by a factor of 1.6 only, Table 1). Moreover, the photochemically active UV irradiance (*3, 6, 12, 26*) remained unchanged at 4.2−4.9% of the global irradiation throughout the year (SI Table S2). Finally, the UV normalized on-board formation rates, are significantly higher in spring−summer as compared to winter (Table 1, SI Figure S4), thus indicating that an environmental parameter other than solar irradiation is responsible for the H_2O_2 seasonality.

H_2O_2 Loss Pathways−Dark Decay and Downward Mixing. Since both the on-board H_2O_2 photoformation (SI Figure S4) and the surface water H_2O_2 accumulation (Figure 1a and SI Figure S2) are net rates, H_2O_2 loss processes via decomposition and mixing to depth have to be considered. Starting with H_2O_2 decomposition, numerous samples from cruises and photochemical experiments ($n = 80$) were incubated for 10−48 h in darkness after which the remaining H_2O_2 was recorded (SI Table S3). Not having measured the decay kinetics nor determined the reaction order, H_2O_2 half-life can be evaluated with precision only for several fortuitous samples where exactly half of the initial H_2O_2 decayed during this time, while in other cases, an upper or lower limit was estimated (SI Table S3). This analysis revealed that H_2O_2 half-life in the Gulf is in the order of 1−2 days for September and December incubations and 16−24 h for April and October incubations (SI Table S3). In May, faster decays were seen, possibly in association with a bloom of Synechococcus (filtration through 0.2 μm resulted in much slower decays, Table S3). Our estimated spring−summer half-lives are typical to those found in other coastal environments such as Biscayne Bay or Chesapeake Bay (~0.5 d^{-1}; refs *3, 5)*, whereas the winter half-life approach those found in open ocean (typically 1−4 d^{-1}; refs *6, 11, 13*,). As the seasonal changes in H_2O_2 half-life show a different pattern than that of its photoformation rates, they at best strengthen the previous statements. In practice, a half-life of 16−24 h implies a minimal effect on net formation rates in 3 h long on-board experiments (Figure 3 and SI Figure S4). It is important to note that due to methodological limitations, we studied H_2O_2 decay in the dark only, whereas reactions with other photocemically generated species such as Fe(II), present in the Gulf during the day time only (*22*), may accelerate the loss of H_2O_2 in the light as discussed later.

Another loss pathway for surface H_2O_2 is its mixing with low H_2O_2 deep waters. Physical processes such as wind-induced mixing of the surface layer, convective mixing, and eddy diffusivity, are important players in H_2O_2 vertical distribution and diurnal variations (*11, 12*). For example, the exponential decline of H_2O_2 concentrations with depth which is weaker (i.e., it penetrates deeper) than that of light (either UV or PAR, Figure 1b), is indicative of a net downward mixing. Similarly, the sharp decline in surface [H_2O_2] in the evening (SI Figure S2) most likely results from cooling and sinking of surface waters (*12*). Can the lower midday surface [H_2O_2] in winter simply result from stronger mixing in this season? We think that the answer is no and that while physical processes in the Gulf surely vary with time, they play a minor role (if any) in the seasonal changes of the surface [H_2O_2]. This statements is based on the tight linear correlation ($R^2 = 0.95$) found between the surface noon H_2O_2 concentrations and the simultaneous on-board net photoformation rates (SI Figure S5). The fact that both winter and spring−summer data follow the same trend indicates that short-term (sunrise-noon) mixing processes operate on the same scale for both seasons. In support of this notion, a development of a daily thermocline was observed in most cruises, possibly somewhat restraining surface water mixing in midday hours.

Water Composition. Based on the above, the higher spring−summer UV normalized on-board net H_2O_2 formation rates (Table 1, SI Figure S4) represent a change in the water characteristics. This idea was confirmed in concurrent in-situ incubations in quartz tubes with winter and spring waters, resulting in 1.6 ± 0.5 times faster net H_2O_2 photoformation in April as compared to January (SI Figure S7). This and the moderate increase in the water temperature in spring (SI Table S1, 1−2 °C), rule out temperature as a variable influencing H_2O_2 seasonality. Seasonal variations in trace metal abundance or reactivity can not account for these changes, as they were found to have no (Cu) or small (Fe) effect on H_2O_2 photoformation (see below) and iron concentrations in the surface waters were rather constant throughout the year (Table 1). On the other hand, higher spring−summer CDOM concentrations may support higher H_2O_2 formation rates. In the absence of runoff, phytoplankton blooms and their demise in spring−summer is likely the dominant source of organic matter to the Gulf. In accordance with this, we found statistically higher spring−summer CDOM concentrations (reported as absorbance coefficient at 355 nm − α_{355}) than winter values (Table 1; p value = 0.0098). A relationship between H_2O_2 photoformation and CDOM was reported previously, but for CDOM from terrestrial sources (*3, 25, 27*). These findings are one of the only reports on such a relationship with CDOM generated (most likely) by phytoplankton.

Role of Superoxide and Trace Metals in H_2O_2 Photoformation. Recently, we have characterized a highly dynamic photomediated redox cycle of iron in the Gulf, that maintains midday steady state Fe(II) of 50−200 pM (*22*). Assuming that these redox transformations influence and are influenced by superoxide and H_2O_2 (as well as oxygen) we simultaneously studied the photodynamics of all three species. We focus here mostly on the data related to H_2O_2 photoformation, and further explore the Fe(II) and O_2^- dynamics in another paper (Shaked, in prep).

Trace Metals and Organic Matter As Sinks for Superoxide. An insightful approach for assessing O_2^- reactions with trace elements, involves the addition of O_2^- spikes to natural and DTPA containing seawater (and/or amended with metals) and the examination of their decay kinetics according to eq 7 (*18, 21, 28*);

$$-\frac{d[O_2^-]}{dt} = 2k_D[O_2^-]^2 + \sum k_M[M]_x[O_2^-] + k_{org}[O_2^-] \quad (7)$$

Where the first term is uncatalyzed second order dismutation (*16*), the second term is metal catalyzed dismutation (which is eliminated by the addition of DTPA (*17*)), and the third term is organic matter catalyzed dismutation (*18*). Unlike most other studies, we applied subnanomolar to nanomolar O_2^- spikes (0.2−10 nM O_2^-), similar to [O_2^-] levels measured in our experiments (see below). At these low concentrations and in the presence of other large O_2^- sinks the uncatalyzed dismutation is negligible and the overall decay kinetics is expected to follow pseudofirst order as was indeed observed in all our treatments (Figure 3, SI Table S4). O_2^- decay rates in natural seawater, expressed as the overall first order decay constant k_{obs} were 0.025−0.045 s^{-1} (Figure 2; SI Table S4), within the range of Southern Ocean values of k_{obs} = 0.004−0.073 s^{-1} (*28*), but lower than those found in high CDOM coastal waters (*18*). O_2^- half-life in the Gulf of Aqaba calculated from these decays ranges from 15 to 28 s. Significantly slower decays were found upon complexation of the ambient metals by DTPA in a O_2^- nonreactive form with k_{obs} = 0.004−0.015 s^{-1}, indicating that reactions with metals are the major O_2^- sinks in these waters (Figure 2, SI Table S4). O_2^- decay kinetics in the presence of DTPA also obey pseudofirst order (rather than second order, eq 7), suggesting that reactions between organic matter and O_2^- prevail under those conditions. Such reactions were studied in coastal waters with high terrestrial impact by Goldstone

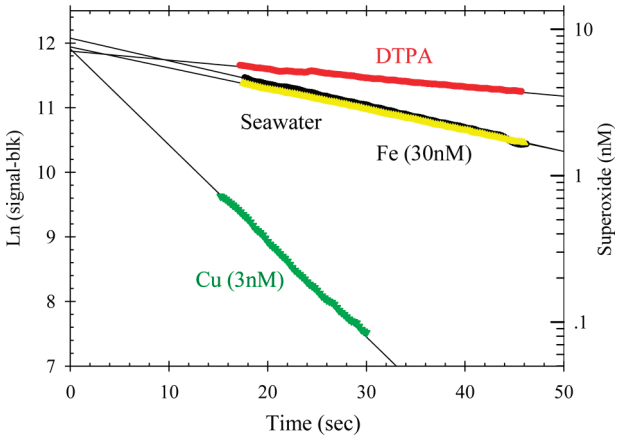

FIGURE 2. Decay kinetics of superoxide spikes (~8 nM) in ambient seawater, in metal amended seawater, 30 nM Fe and 3 nM Cu, and in metal-chealated seawater (150 μM DTPA, labeled on the graph). Linear decays in a log−linear plot, indicative of a pseudofirst order process were found for all treatments. The precise match between the added [O_2^-] and the initial [O_2^-] obtained from the back-extrapolation further validate the calculated decay constants (see SI for more details).

and Volker (*18*) who obtained a correlation between the CDOM absorption at 300 nm and the rate of O_2^- decay in the presence of DTPA (expressed as k_{org} rather than k_{obs}, eq 7). Substituting the Gulf CDOM absorption of 0.19−0.43 m^{-1} at 300 nm into their relationships yields $k_{org} = 0.1\ s^{-1}$, which is an order of magnitude faster than the k_{org} of 0.004−0.015 s^{-1} found here (Figure 2, SI Table S4). This discrepancy, recently reported also in the Southern Ocean (*28*), may suggest that marine CDOM produced by phytoplankton (which is likely the case in this arid environment) is far less reactive with O_2^- than CDOM from terrestrial sources. The added copper (3 nM) was highly reactive with O_2^- resulting in a $k_{obs} = 0.13−0.28\ s^{-1}$ (Figure 2, SI Table S4, at 6 nM Cu the O_2^- decay was too fast to follow). On the other hand, O_2^- decay with added iron (30 nM), was similar to that of ambient seawater, indicating that it did not interact with O_2^- (Figure 2, SI Table S4). The reactivity of the added metals with O_2^- may not represent that of the ambient dissolved Fe (4−6 nM, Table 1) and dissolved Cu (~2 nM (*29*)), but in the absence of speciation data, this issue remains enigmatic. Nonetheless, the trends observed here together with published constants (*16*−*20*) and the recently reported stronger effect of Cu than Fe on O_2^- decay in the Southern Ocean (*28*), all suggest a major role for Cu in O_2^- decay in ambient Gulf water.

H_2O_2 Photoformation Rates with Added SOD, Cu, and Fe. To examine whether trace metals (and organic matter to a lesser degree) interact catalytically with O_2^- (reactions 3 and 4), noncatalytically (reaction 3 or 4), or follow other pathways (reactions 5 or 6) we studied H_2O_2 photoformation rates in surface incubations of seawater amended with SOD, iron and copper (Figure 3). As with our other experiments, the net H_2O_2 formation was highly linear with time and cumulative UV flux (Figure 3a). Highly reproducible net H_2O_2 formation rates were observed throughout the year with typical values of 20−35 nM/h or 1−1.4 nM $m^2\ W^{1-}\ h^{-1}$ (Figure 3). We corrected for values of H_2O_2 formation in the dark which ranged between 2 and 9 nM/h (with the higher values found with added metals, Figure 3a, SI Figure S11). Dark H_2O_2 decay, followed for two days after the experiments, was slow ($t_{1/2}$ = 1−2 days) and independent of metal addition or complexation (SI Figure S10). We can thus safely state that the dark decay plays no role in these short (~2−3 h) photoexperiments (i.e., that gross and net rates are equal). Increasing concentrations of the enzyme superoxide dismutase (SOD; 50, 100, 150, and 250 nM) and copper (3 and 6 nM), had no effect on net H_2O_2 photoformation (Figure 3a, SI Figure S11). The lack of response to these high levels of catalysts implies that all the photoformed O_2^- is already converted to H_2O_2 via catalytic activity in their absence. Since metals are the major O_2^- sink in these waters (Figure 2), this finding further suggests that H_2O_2 in the Gulf is generated by trace metal catalyzed disprortionation of O_2^-. Our data differ from that of Patsane and Zika (*15*), who estimated by adding SOD to coastal waters (from Biscayne Bay, Miami) that up to 40% of O_2^- sink pathways do not generate H_2O_2. Iron, added at concentrations of 12−50 nM (in three different experiments), was found to moderately slow the net H_2O_2 formation (Figure 3b). This effect most likely resulted from H_2O_2 consumption during the oxidation of Fe(II) via the Fenton reaction (eq 6), as explained below.

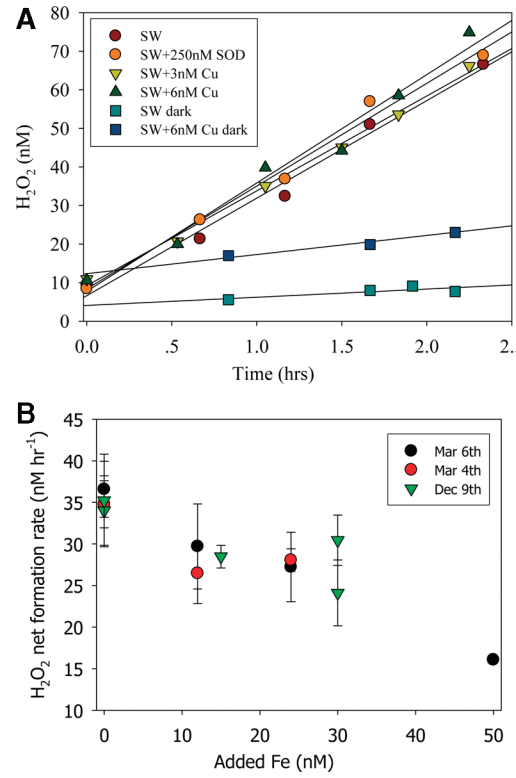

FIGURE 3. H_2O_2 photoformation in ambient (and amended) seawater from the Gulf of Aqaba that were incubated in beakers under midday natural irradiation. (A). H_2O_2 accumulation in seawater and with additions of SOD (250 nM) and copper (3 and 6 nM) as labeled on the plot. H_2O_2 accumulation in non illuminated samples was assessed for all treatments (noted as dark and shown for representative treatments only). Linear regressions, all with $R^2 > 0.98$ are plotted as thin lines. Additional treatments and replicates are presented in SI Figure S11. (B). Net, dark corrected H_2O_2 formation rates in seawater amended with increasing iron concentration. Rates are from 2−3 h long experiments with different seawater on three separate dates. Error bars are drawn from the error on the slope of [H_2O_2] versus time.

Superoxide and Fe(II) Dynamics in Photoexperiments. The above conclusions were reaffirmed by simultaneously measuring H_2O_2 formation and O_2^- and Fe(II) photodynamics in the same vials. A characteristic pattern was observed where both O_2^- and Fe(II) rapidly increased upon exposure to the sun, obtained a stable steady state and promptly decayed in the dark (Figures 4 and SI S9). The different aspects of these experiments are described elsewhere (Shaked, in prep), while here we focus on data related to the two tentative conclusions raised in the former sections: (1) Metal (probably Cu) catalyzed O_2^- dismutation governs H_2O_2 formation in the

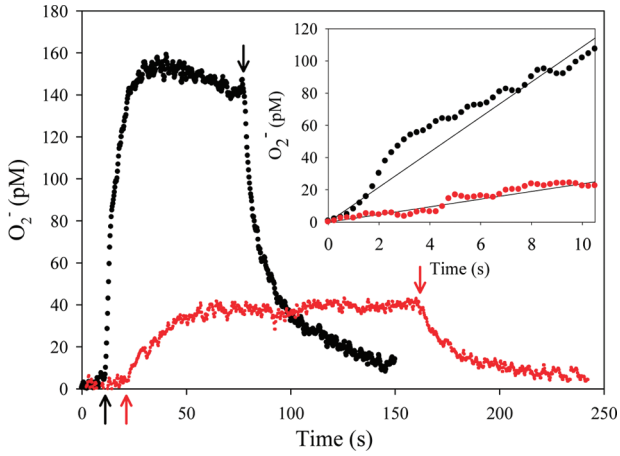

FIGURE 4. Representative superoxide photodynamics experiment, similar to those obtained simultaneously with H_2O_2 (Figure 3) and Fe(II) (Figure S9) in ambient seawater (black dots) and with addition of 3 nM Cu (red dots). Background values were measured first in the dark followed by an exposure to sunlight (upward arrows), where O_2^- formation rates were determined (initial formation rates are shown in insert). Once stable steady state O_2^- concentrations was achieved the sample was covered (downward arrows) and O_2^- decay was followed. The resulting formation rates, steady state concentrations and pseudo first order decay constants for this and other experiments are shown in SI Table S4. Note that the concentrations are not corrected for the decay in the FeLume tubing which might be significant.

Gulf of Aqaba and (2) Fe(II) oxidation by H_2O_2 moderately lowers the net H_2O_2 photoformation in Fe ammended and natural waters.

Superoxide show a linear build-up during the first 4−10 s following irradiation ($R^2 > 0.95$), and its photoformation rates range between 3 and 25 pM s^{-1} (Figure 4, SI Table S4). We note that this method of evaluating O_2^- formation rates is very inaccurate as the choice of formation time is subjective and the inclusion or exclusion of even 1 s (four data points) may lead to large variations in the resulting rates. Constrains on these rates can be obtained using other data collected during the experiments. At equilibrium, O_2^- formation should equal its decay, and the rate of formation can be calculated by multiplying the $[O_2^-]_{s.s}$ by its first order decay constant, k_{obs} (*18, 21, 28*). This calculation with $[O_2^-]_{s.s} = 100-160$ pM and $k_{obs} = 0.03-0.07$ s^{-1} yields rates of 3−15 pM s^{-1} that agree well with those evaluated from the initial build-up (SI Table S4). The ratio of O_2^- formation (3−25 pM s^{-1}) to H_2O_2 formation (4−10 pM s^{-1}) may represent the expected 2:1 dismutation ratio, although given the range in the rates a 1:1 ratio can not be ruled out. The comparison between the rates is further complicated by the large differences in the resolution of sampling (O_2^- formation is measured every 0.25 s for 10 s while H_2O_2 is sampled every 20 min for 2 h). Nonetheless, as the data presented so far strongly suggests that H_2O_2 is formed via metal catalyzed O_2^- dismutation, we take the resulting reasonable O_2^- to H_2O_2 formation ratio to indicate that these challenging O_2^- measurements are meaningful. While some modifications on the O_2^- values are required (not corrected for decay in tubing) and it remains to be seen if they represent in-situ values, they still are one the first to be made in seawater. Our photogenerated $[O_2^-]_{s.s}$ of ∼100 pM agrees well with that estimated for sunlit coastal waters of 10−100 pM (*18*), and our O_2^- photoformation rates of 3−25 pM s^{-1} are within the range of 2−200 pM s^{-1} reported previously (*18, 30*). Similar to the O_2^- spike decay (Figure 2), Fe addition had no influence on $[O_2^-]_{s.s}$ or formation rates (SI Table S4). It is yet unclear if the lack of reactivity with O_2^- of the added iron (which probably precipitated out), is also shared by the ambient iron present at 4−12 nM (Table 1). If so, and contrary to our assumption (*22*), then direct photolysis of organic iron complexes (that were not yet characterized) has to account for the observed high Fe(II) photoformation rates (SI Figure S9 (*22*)). Copper (3nM), on the other hand, was so reactive with O_2^- that it suppressed the ambient water $[O_2^-]_{s.s}$ from 100−160 pM to 20−40 pM and even lowered the initial O_2^- formation rates (Figure 4).

Steady state Fe(II) concentrations of ∼200 and ∼400 pM were measured in ambient seawater and with added Fe (30 nM), respectively, and were stable with time (SI Figure S9). Fe(II) oxidation rates were similar in both treatments (SI Figure S9), with a pseudo first order constant $k_{obs} = 0.01-0.02$ s^{-1} (obtained also with Fe(II) spikes, see ref (*22*) for details). Hence, an additional Fe(II) oxidation rate of 7−14 nM hr^{-1} (200 pM × 0.01−0.02 s^{-1} × 3600 s/h), occurs in the Fe added treatment and may be mediated, at least in part, by H_2O_2. This calculation can accommodate the 7 nM hr^{-1} slower net H_2O_2 formation rate observed with added iron (Figure 4b), a process that may also influence H_2O_2 formation in situ. Based on published oxidation constants (*2, 31*) H_2O_2 at concentrations as low as 30−50 nM competes with oxygen and O_2^- on Fe(II) oxidation. Hence, the in situ measured Fe(II) oxidation rates of 2−8 nM hr^{-1} (*22*), is likely to moderately lower H_2O_2 during spring−summer when it exceeds 30−50 nM (Table 1; SI Figure S3).

Acknowledgments

We acknowledge the valuable contribution of many colleagues and students to this study: Muriel Dray, Hagar Lis, Eldad Saragosti, Maxim Rubin, Asaph Rivlin, and Itzik Lerer for help with measurements and field work; Gal Dishon and Félix López Figueroa for providing light measurements, the Israel National Monitoring Program (NMP) at the Northern Gulf of Aqaba (Amatzia Genin, Yonathan Shaked, Muriel Dray, Tanya Rivlin, Inbal Ayalon) for sharing their cruises and data; and Yigal Erel, FranÇois Morel, and four anonymous reviewers for providing constructive comments on the manuscript. This research was supported (in part) by the Israel Science Foundation (grant no. 933/07) and the Hebrew University Moshe Shilo Minerva Center for Marine Biogeochemistry.

Supporting Information Available

Complete descriptions of the study site, experimental methods, and an-abbreviated chemicals used. This material is available free of charge via the Internet at http://pubs.acs.org.

Literature Cited

(1) Zafiriou, O. C.; Joussot-Dubien, J.; Zepp, R. G.; Zika, R. G. Photochemistry of natural waters. *Environ. Sci. Technol.* **1984**, *18*, 358A–371A.

(2) Moffett, J. W.; Zika, R. G. Reaction kinetics of hydrogen peroxide with copper and iron in seawater. *Environ. Sci. Technol.* **1987**, *21*, 804–810.

(3) Cooper, W. J.; Shao, C.; Lean, D. R. S.; Gordon, A. S.; Scully J. F. E. Factors affecting the distribution of H_2O_2 in surface waters. In *Environmental Chemistry of Lakes and Reservoirs*; Baker, L. A. , Ed.; American Chemical Society: Washington, DC, 1994; pp 391−422.

(4) Pettine, M.; Millero, F. J. Effect of metals on the oxidation of As(III) with H_2O_2. *Mar. Chem.* **2000**, *70*, 223–234.

(5) Petasne, R. G.; Zika, R. G. Hydrogen peroxide lifetimes in south Florida coastal and offshore waters. *Mar. Chem.* **1997**, *56* (3−4), 215–225.

(6) Yuan, J.; Shiller, A. M. The distribution of hydrogen peroxide in the center Atlantic Ocean. *Deep-Sea Res. II* **2001**, *48*, 2947–970.

(7) Moffett, J. W.; Zafiriou, O. C. An investigation of hydrogen peroxide chemistry in surface waters of Vineyard Sound with $H_2{}^{18}O_2$ and $18O_2$. *Limnol. Oceanogr* **1990**, *35*, 1221–1229.

(8) Wong, G. T. F.; Dunstan, W. M.; Kim, D. B. The decomposition of hydrogen peroxide by marine phytoplankton. *Oceanologica Acta* **2003**, *26*, 191–198.
(9) Szymczak, R.; Waite, T. D. Generation and decay of hydrogen peroxide in estuarine waters. *Aust. J. Mar. Freshwater Res.* **1988**, *39* (3), 289–299.
(10) Steigenberger, S.; Croot, P. L. Identifying the processes controlling the distribution of H_2O_2 in surface waters along a meridional transect in the eastern Atlantic. *Geophys. Res. Lett.* **2008**, *35*, L03616, DOI: 03610.01029/02007GL032555.
(11) Yuan, J.; Shiller, A. M. The distribution of hydrogen peroxide in the southern and central Atlantic Ocean. *Deep-Sea Res. II* **2001**, *48*, 2947–2970.
(12) Obernosterer, I.; Ruardij, P.; Herndl, G. J. Spatial and diurnal dynamics of dissolved organic matter (DOM) fluorescence and H_2O_2 and the photochemical oxygen demand of surface water DOM across the subtropical Atlantic Ocean. *Limnol. Oceanogr* **2001**, *46* (3), 632–643.
(13) Avery, Jr, G. B.; Cooper, W. J.; Keiber, R. J.; Willey, J. D. Hydrogen peroxide at the Bermuda Atlantic Time Series Station: Temporal variability of seawater hydrogen peroxide. *Mar. Chem.* **2005**, *97*, 236–244.
(14) Palenik, B.; Morel, F. M. M. Dark production of H_2O_2 in the Sargasso Sea. *Limnol. Oceanogr.* **1988**, *33*, 1606–1611.
(15) Petasne, R. G.; Zika, R. G. Fate of superoxide in coastal sea water. *Nature* **1987**, *325*, 516–518.
(16) Zafiriou, O. C. Chemistry of superoxide ion (O_2^-) in seawater. I. pK_{asw}* (HOO) and uncatalysed dismutation kinetics studied by pulse radiolysis. *Mar. Chem.* **1990**, *30*, 31–43.
(17) Zafiriou, O. C.; Voelker, B. M.; Sedlak, D. L. Chemistry of the superoxide radical (O_2^-) in seawater: Reactions with inorganic copper complexes. *J. Phys. Chem. A* **1998**, *102* (28)), 5693–5700.
(18) Goldstone, J. V.; Voelker, B. M. Chemistry of superoxide radical in seawater: CDOM associated sink of superoxide in coastal waters. *Environ. Sci. Technol.* **2000**, *34*, 1043–1048.
(19) Voelker, B. M.; Sedlak, D. L.; Zafiriou, O. C. Chemistry of superoxide radical in seawater: reactions with organic Cu complexes. *Environ. Sci. Technol.* **2000**, *34*, 1036–1042.
(20) Voelker, B. M.; Sedlak, D. L. Iron reduction by photoproduced superoxide in seawater. *Mar. Chem.* **1995**, *50*, 93–102.
(21) Rose, A. L.; Webb, E. A.; Waite, T. D.; Moffett, J. W. Measurement and implications of nonphotochemically generated superoxide in the equatorial Pacific Ocean. *Environ. Sci. Technol.* **2008**, *42* (7), 2387–2393.
(22) Shaked, Y. Iron redox dynamics in the surface waters of the Gulf of Aqaba, Red Sea. *Geochim. Cosmochim. Acta* **2008**, *72*, 1540–1554.
(23) Zhou, M.; Diwu, Z.; Panchuk-Voloshina, N.; Haugland, R. P. A stable nonfluorescent derivative of resorufin for the fluorometric determination of trace hydrogen peroxide: Applications in detecting the activity of phagocyte NADPH oxidase and other oxidases. *Anal. Biochem.* **1997**, *253*, 162–168.
(24) Kirk, J. T. O. *Light and Photosynthesis in Aquatic Ecosystems*; Cambridge University Press: Cambridge, 1994.
(25) Herut, B.; Shoham-Frider, E.; Kress, N.; Fiedler, U.; Angel, D. L. Hydrogen peroxide production rates in clean and polluted coastal marine waters of the Mediterranean, Red and Baltic Seas. *Mar. Pollut. Bull.* **1998**, *36* (12), 994–1003.
(26) Gerringa, L. J. A.; Rijkenberg, M. J. A.; Timmermans, K. R.; Buma, A. G. J. The influence of solar ultraviolet radiation on the photochemical production of H_2O_2 in the equatorial Atlantic Ocean. *J. Sea Res.* **2004**, *51*, 3–10.
(27) Cooper, W. J.; Zika, R. G.; Petasne, R. G.; Plane, J. M. C. Photochemical formation of H_2O_2 in natural waters exposed to sunlight. *Environ. Sci. Technol.* **1988**, *22*, 1156–1160.
(28) Heller, M. I; Croot, P. L. Superoxide decay kinetics in the southern ocean. *Environ. Sci. Technol.* **2010**, *44*, 191–196.
(29) Chen, Y.; Paytan, A.; Chase, Z.; Measures, C.; Beck, A. J.; Sañudo-Wilhelmy, S. A.; Post, A. F. Sources and fluxes of atmospheric trace elements to the Gulf of Aqaba, Red Sea. *J. Geophys. Res., [Atmos.]* **2008**, *113*, D05306.
(30) Micinski, E.; Ball, L. A.; Zafiriou, O. C. Photochemical oxygen Activation—Superoxide radical detection and production-rates in the eastern Caribbean. *J. Geophys. Res., [Oceans]* **1993**, *98* (C2), 2299–2306.
(31) González-Dávila, M; Santana-Casiano, J. M.; Millero, F. J. Competition Between O_2 and H_2O_2 in the Oxidation of Fe(II) in Natural Waters. *J. Solution Chem.* **2006**, *35* (1), 95–111.
(32) Croot, P. L.; Laan, P.; Nishioka, J.; Strass, V.; Cisewski, B.; Boye, M.; Timmermans, K.; Bellerby, R.; Goldson, L.; de Baar, H. J. W. Spatial and Temporal distribution of Fe(II) and H_2O_2 during EISENEX, an open ocean mesoscale iron enrichment. *Mar. Chem.* **2005**, *95*, 65–88.

ES902343Y